Thin Solid Films 519 (2010) 251–258

Contents lists available at ScienceDirect

Thin Solid Films

journal homepage: www.elsevier.com/locate/tsf

Effects of heat treatment on the microstructure of amorphous boron carbide coating deposited on graphite substrates by chemical vapor deposition ☆

Siwei Li [a,b], Bin Zeng [a], Zude Feng [a,*], Yongsheng Liu [b], Wenbin Yang [b], laifei Cheng [b], Litong Zhang [b]

[a] Fujian Key Laboratory of Advanced Materials, College of Materials, Xiamen University, Xiamen, 361005, China
[b] National Key Laboratory of Thermostructure Composite Materials, Northwestern Polytechnical University, Xi'an 710072, China

ARTICLE INFO

Article history:
Received 29 August 2009
Received in revised form 21 June 2010
Accepted 16 August 2010
Available online 21 August 2010

Keywords:
Amorphous boron carbide
Annealing
Microstructure
Epitaxial growth
Chemical vapor deposition

ABSTRACT

A two-layer boron carbide coating is deposited on a graphite substrate by chemical vapor deposition from a $CH_4/BCl_3/H_2$ precursor mixture at a low temperature of 950 °C and a reduced pressure of 10 KPa. Coated substrates are annealed at 1600 °C, 1700 °C, 1800 °C, 1900 °C and 2000 °C in high purity argon for 2 h, respectively. Structural evolution of the coatings is explored by electron microscopy and spectroscopy. Results demonstrate that the as-deposited coating is composed of pyrolytic carbon and amorphous boron carbide. A composition gradient of B and C is induced in each deposition. After annealing, B_4C crystallites precipitate out of the amorphous boron carbide and grow to several hundreds nanometers by receiving B and C from boron-doped pyrolytic carbon. Energy-dispersive spectroscopy proves that the crystallization is controlled by element diffusion activated by high temperature annealing, after that a larger concentration gradient of B and C is induced in the coating. Quantified Raman spectrum identifies a graphitization enhancement of pyrolytic carbon. Transmission electron microscopy exhibits an epitaxial growth of B_4C at layer/layer interface of the annealed coatings. Mechanism concerning the structural evolution on the basis of the experimental results is proposed.

1. Introduction

Boron carbide is an important non-metallic material with outstanding hardness, excellent mechanical, thermal and electrical properties. It is also a good barrier against oxygen diffusion [1]. In recent years, boron carbide coatings have been developed as a component of SiC-based ceramic matrix composites (CMC-SiC) to improve the high temperature durability of the composites by providing a self-healing and oxidation resistant functionality [2]. The coatings are widely prepared by chemical vapor deposition (CVD) due to the better controlled deposition process and the compactly deposited coating structure [3–11]. Many of the experimental researches are carried out using cold-wall reactors at a high temperature (T>1100 °C) and either at atmospheric [12–14] or reduced pressure [10,15,16]. Recently, amorphous boron carbide (α-B_4C) coatings are prepared by relatively simple and controllable technologies using a hot-wall reactor at low temperatures (800–1050 °C) and reduced pressures. Studies are carried out on the law of kinetic and that of the thermodynamics to explore the deposition mechanisms [17–19]. However, CVD is more complicated than a balanced reaction and produces various compositions that can hardly be measured by calculated phase diagrams. More efforts should be made to understand the deposited structure.

Relationship between the microstructure and the physicochemical properties of CVD boron carbide is of great interest for engineering applications. Many investigations are performed on crystalline materials [14–16], few exceptions are about amorphous coatings [20,21]. However, studies rarely concern the microstructural evolution of α-B_4C coating after annealing at high temperatures in an inert atmosphere. It's known that CVD α-B_4C is always designed as inner matrix coatings to improve the oxidative stability of CMC-SiC through the healing of micro-sized defects with oxides. Nevertheless, the coatings are also load bearing units and strength transmission components which always serve at high temperatures in oxygen free environments. The thermal stability of the coating structure influences the mechanical behavior of CMC-SiC to a certain extent.

The present work focuses on microstructural evolution of CVD α-B_4C coatings annealed in Ar under a range of a high temperature from 1600 °C to 2000 °C. Two layers of α-B_4C are prepared to investigate the structural change at the layer/layer interface and to explore annealing-induced differences from that of the single layer. Results and discussions are helpful to facilitate the application of the CVD α-B_4C as different components of matrix coatings used for strengthening, toughening and even self-healing of CMC-SiC.

2. Experimental procedure

Coatings are prepared in a vertical hot-wall reactor with 200 mm inner diameter at 950 °C and a total pressure of 10 kPa. In the CVD process, boron trichloride ($BCl_3 \geq 99.99$ vol.% and iron ≤ 10 ppm) is

☆ Supported by the National Natural Science Foundation of China (Grant No. 50532010 and No. 90405015).
* Corresponding author.
E-mail address: zdfeng@xmu.edu.cn (Z. Feng).

0040-6090/$ – see front matter © 2010 Elsevier B.V. All rights reserved.
doi:10.1016/j.tsf.2010.08.099

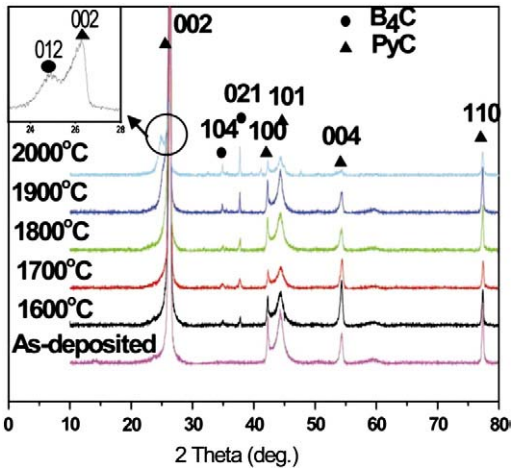

Fig. 1. XRD patterns show precipitation and grain growth of B_4C crystallites (circular dots) out of the PyC (triangular dots) phase after annealing from 1600 °C to 2000 °C.

used as the boron source mixed with a dilution gas of hydrogen ($H_2 \geq 99.999$ vol.%). Methane ($CH_4 \geq 99.95$ vol.%) is used as carbon source and argon (Ar ≥ 99.99 vol.%) is used as carrier gas. The total pressure in the reaction vessel is measured using a pressure transducer and the flow rates of the gases are measured and regulated by mass flow meters. The measured flow rates of BCl_3, H_2, CH_4, and Ar are 500 cm^3/min, 550 cm^3/min, 100 cm^3/min, and 500 cm^3/min, respectively. The first deposition is performed for 30 h on graphite substrates. Then, the coated substrates are cooled to room temperature. The second deposition is operated with unchanged parameters on the firstly deposited coatings to fabricate a two-layer structure. After that, the two-layer coatings are exposed in argon (Ar ≥ 99.99 vol. %) for 2 h at 1600 °C, 1700 °C, 1800 °C, 1900 °C and 2000 °C, respectively.

Phases existing in the coating are identified using an X-ray diffractometer (XRD, X'pert PRO). Chemical bonding states of boron and carbon elements are analyzed by X-ray photoelectron spectroscopy (XPS, PHI Quantum 2000). In order to eliminate the interference of substrates, all the deposited coatings used in XRD and XPS tests should be removed from the graphite substrate and grinded into powder. Morphologies of the coating are characterized using scanning electron microscopy (SEM, XL30 ESEM-TMP) Compositional change is explored by windowless energy-dispersive spectroscope (EDS, EDAX) equipped on SEM. TEM observations (containing bright field (BF) observation and high resolution (HR) observation) are performed using a TECNAI F30 operated at 300 kV. TEM samples are prepared using a precision ion polishing system (Model 691, Gatan). Cross-sectional specimen are glued on the copper ring of 3 mm in diameter, then embedded with G1 epoxy (Gatan), mechanical pre-thinning (Unipol-820, MTI) and dimple grinding (Model 656, Gatan) are performed before ion thinning.

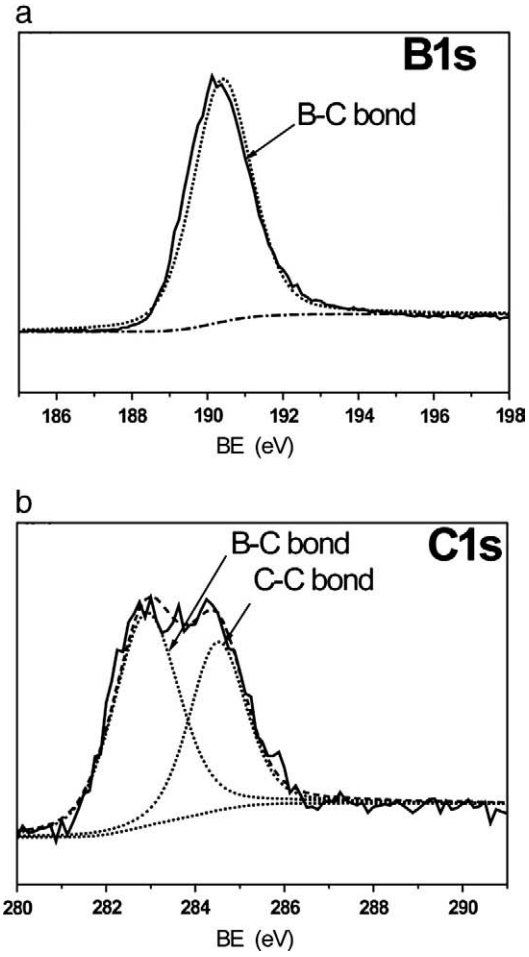

Fig. 2. XPS narrow scanning spectra and fitted results of B1s and C1s of the as-deposited coating after sputter-cleaning of the surface. (a) B–C bond is identified in the B1s spectra, (b) B–C and C–C bonds are identified in the C1s spectra.

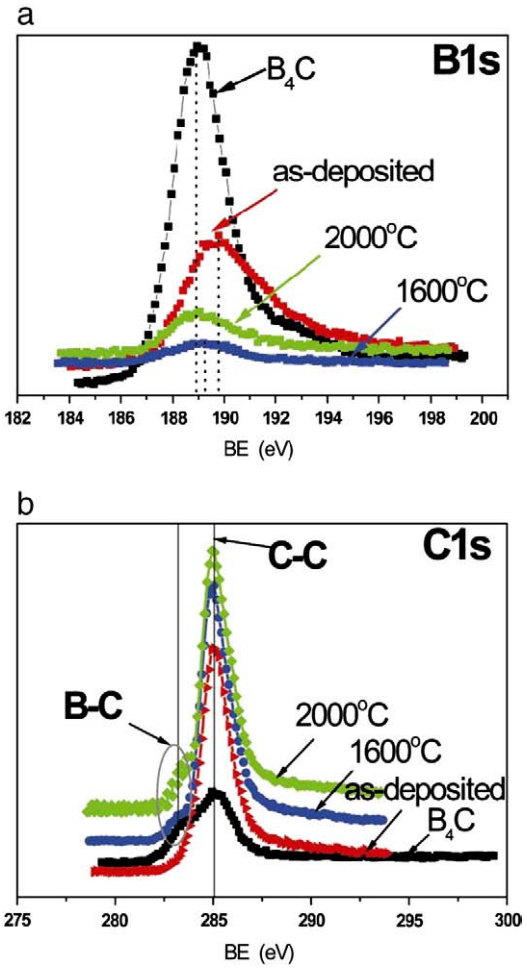

Fig. 3. (a) B1s spectra and (b) C1s spectra of the as-deposited coating (red line), the coating annealed at 1600 °C (blue line) and 2000 °C (green line), and the standard B_4C sample (black line) reveal that the B1s peak shifts to a lower BE side while the C1s peak of the B–C bond emerges with enhancing intensity as elevated annealing temperature. (For interpretation of the references to color in this figure legend, the reader is referred to the web version of this article.)

3. Results and discussion

3.1. Phase analysis

Fig. 1 shows XRD patterns of the coatings before and after annealing. In the pattern of the as-deposited coating, only pyrolytic carbon (PyC) peaks are detected, revealing that the boron containing phase is amorphous. After annealing at 1600 °C, low-intensity peaks of B_4C are identified in addition to that of the PyC, indicating that the as-deposited coating has partly transformed as B_4C crystallites. The higher the temperature rises, the faster the grain grows. More severe crystallization is identified by enhancement of B_4C peaks as the temperature rises up to 2000 °C. Besides, the PyC 002 is clearly broadened after annealing at 1900 °C and divided into two peaks after annealing at 2000 °C. The peak emerged near PyC 002 at 2theta of about 23.6° is identified as B_4C 012. It suggests that more severe crystallization of B_4C and faster growth of lower miller index planes proceed at relatively higher temperatures. A previous study based on the change of d_{002}-spacing reveals that the annealing can remove hydrogen from the coating structure and facilitate densification since the hydrogen within the coating preserves low temperature vapor deposit in its sp2 hybridized form [22,23].

Since XRD cannot give valid information about B in the as-deposited coating, XPS is used to characterize the chemical bonding states of B and C. A few O is detected in addition to B and C in a complete XPS survey of the coating surface. The O is eliminated by Ar ion sputter-cleaning for 10 s. Moreover, the B1s peak shows no shift after sputtering, indicating that no oxidation happened, and the O is just induced as very thin thickness of several nanometers by physical adsorption from the air. Fig. 2 shows deconvolved spectra of the as-deposited coating obtained after Ar ion sputter-cleaning. The B mainly exists as a single type of the B–C bond, while the C mainly exists as C–B bond and C–C bond. The main phases of the as-deposited coating can be identified as PyC and α-B_4C. Previous investigations [24–26] of boron carbide by means of XPS reveal that both B1s and C1s spectra are composed of several different chemical environments. Some of these may result from surface contamination since the samples are exposed to ambient conditions. The others are thought to be intrinsic chemical states of boron carbide originated in its complex structure that presents several non-equivalent sites [27]. Considering the uncertainty in the calibration of each independent spectrum, a standard sample of crystallized B_4C is used as a reference. B1s and C1s spectra of the standard sample, the as-deposited coating and two annealed coatings are put together and compared to explore the structural change induced by heat treatment. Results in Fig. 3 are obtained in the same condition. The B1s peak of the coating annealed at 2000 °C is identified at 188.9 eV, which is the same as the value of the standard sample. While, the B1s peaks of the as-deposited coating and the coating annealed at 1600 °C are observed at 189.7 eV and 189.2 eV, respectively (Fig. 3a). The heat treatment makes the B1s peak shift to the low binding energy (BE) side, which also verifies the formation of the crystallized B_4C [28]. In the C1s spectrum (Fig. 3b), the peak of B–C bond is significantly interfered by that of the C–C bond, the change of C1s (of the B–C bond) induced by annealing is not palpable as that of the B1s. However, an intensity increase of the B–C peak is clearly observed as an elevated annealing temperature. It can be deduced that a boron-doped structure is induced in PyC after CVD and kept as the annealing temperature is relatively low. The structural change caused by doping is imperceptible which can hardly be observed in the XRD pattern but just be detected by the peak shift of XPS. The doped structure is metastable at a higher temperature and apt to impel the grain growth of B_4C by providing B and C to the

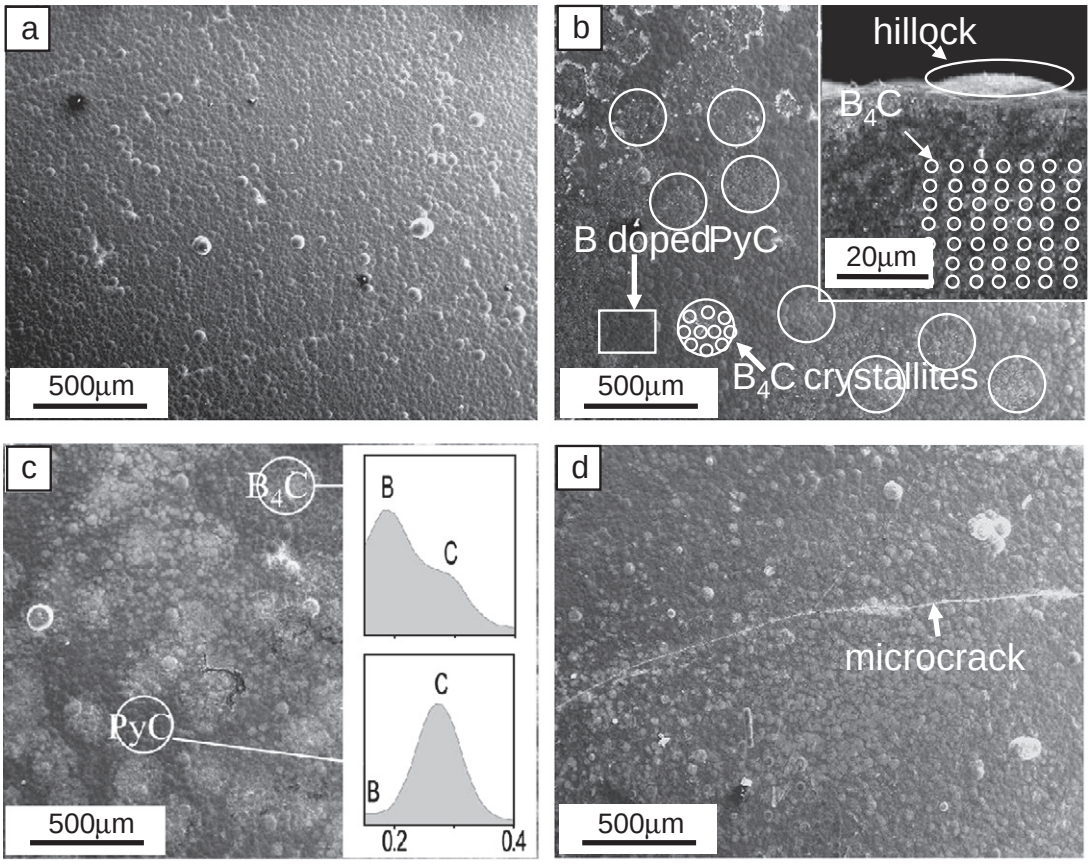

Fig. 4. Surface morphologies of the (a) as-deposited coating, coatings annealed at (b) 1600 °C, (c) 1800 °C and (d) 2000 °C illustrate formation and content enhancement of the crystallized B_4C.

adjacent crystals. The grain boundary migration of B_4C will not stop until the doping B is depleted as there is only PyC left.

3.2. Surface morphology

Surface morphologies of the coatings are characterized by SEM and shown in Fig. 4. The as-deposited coating displays a homogeneous and broccoli-like appearance (Fig. 4a), indicating that the formation and densification of the coating follow a liquid-phase nucleation mechanism. No evident difference is observed between the amorphous structures of PyC and α-B_4C. After annealing at 1600 °C, crystallized B_4C with a lower gray scale than that of the PyC is discovered. However, the B_4C precipitation on the surface of the coating annealed at 1600 °C is macroscopically nonuniform, i.e. large regions of about several tens micrometers of aggregating B_4C crystallites disperse in B-doped PyC, which is most likely caused by the difference of surface energy between the liquid-nucleation induced hillocks and plains. At a relatively low temperature of 1600 °C, the hillocks of relatively higher surface energy facilitate prior formation of the B_4C crystallites. In comparison, the cross-sectional morphology of the coating annealed at 1600 °C (in Fig. 4b) exhibits more uniform distribution of B_4C crystallites at the inner coatings. It proves that the large and the dispersed B_4C regions on the surface are formed by nonuniform precipitation at relatively low annealing temperatures and composed of many early formed nano-grains. Content of the crystallized B_4C shows a notable increase as the annealing temperature rises up to 1800 °C, the EDS spectrum obtained from two regions with different gray scales further confirms the crystallization (Fig. 4c). The free surfaces of all coatings exhibit similar features in addition to microcracks emerged that after annealing at 2000 °C (Fig. 4d). Formation of the microcrack is closely related with the existence of residual stress induced by extrusion and collision of the dramatically grown B_4C crystals.

3.3. Microstructural evolution

Fig. 5 shows the microstructure of the coatings. BF image (Fig. 5a) reveals that the as-deposited coating has a long-range amorphous structure. The three diffraction rings with a weak intensity are identified as the (002), (101) and (004) planes of graphite, which are the characters of the low ordered PyC structure. After annealing at 1600 °C, diffraction rings of B_4C appear in addition to that of the PyC, indicating that B_4C crystallites precipitate out of the amorphous coating, as shown in Fig. 5b. It shows that the structure of the coating

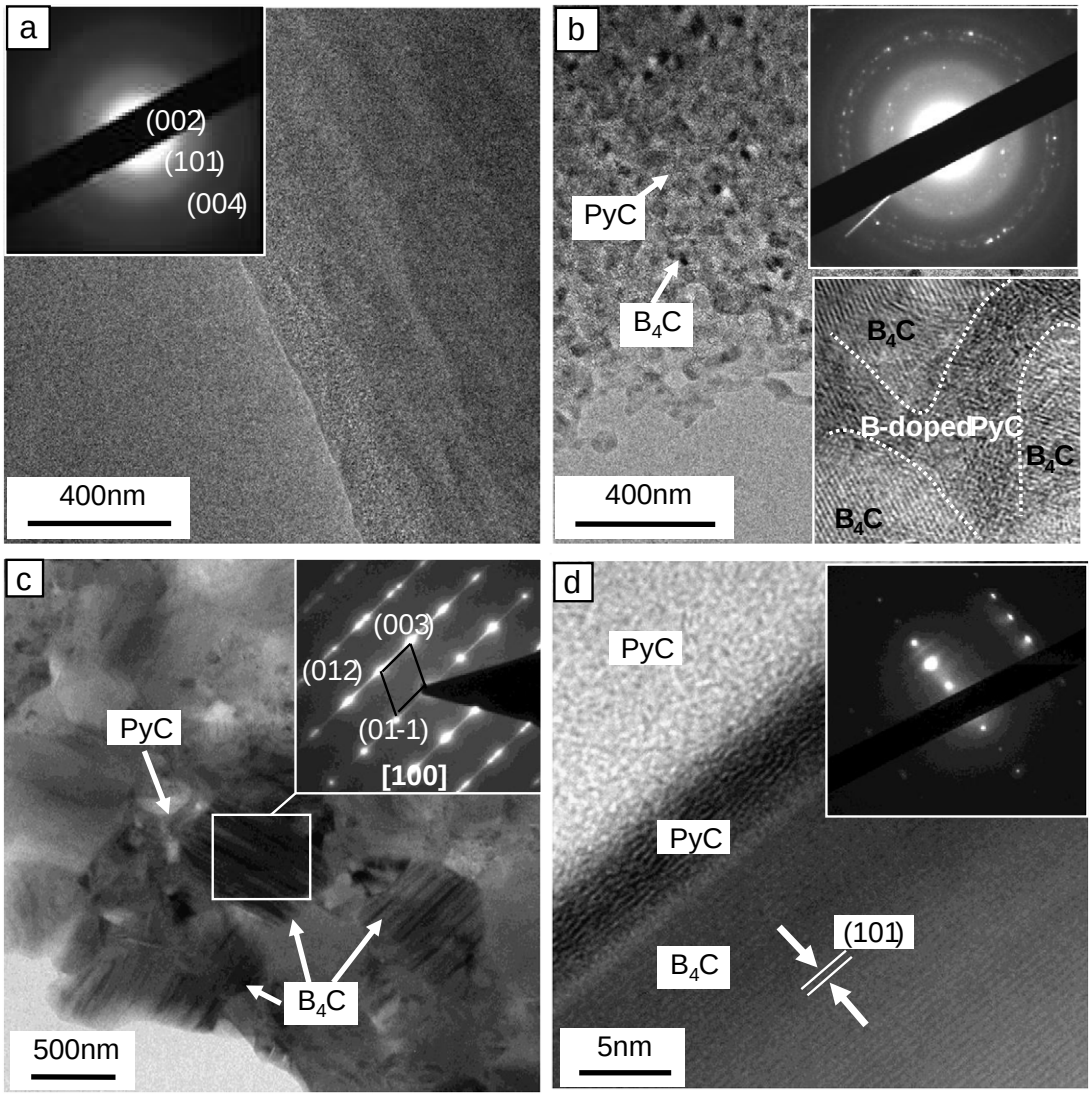

Fig. 5. SAED patterns and BF images of the (a) as-deposited coating, (b) coating annealed at 1600 °C and (c) 2000 °C show the grain growth of B_4C. (d) HR image reveals the epitaxial growth of PyC along the low miller index plane of the B_4C after being annealed at 2000 °C.

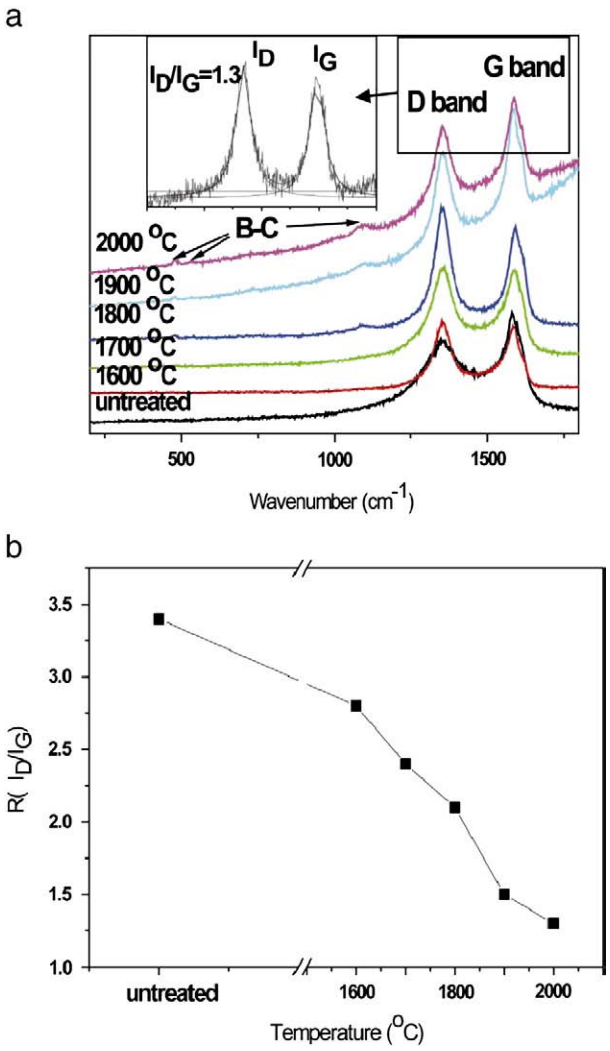

Fig. 6. Graphitization degree of PyC determined by the Raman spectrum. (a) Raman spectrum of the coatings before and after annealing, (b) the change of graphitization degree evaluated by R (the peaks of D bond and G bond are fitted and calculated using the Gaussian model).

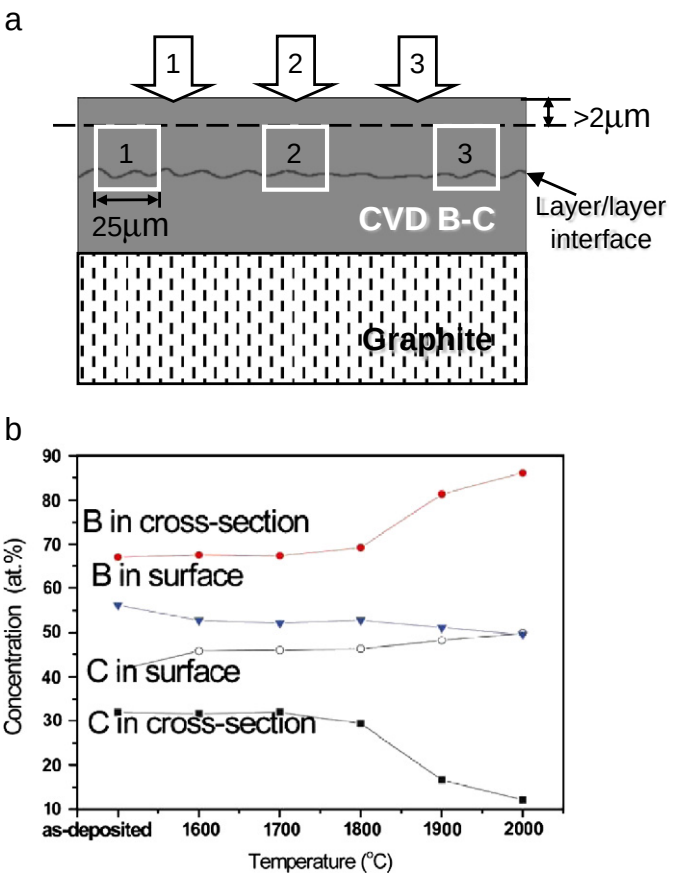

Fig. 8. EDS method and test result of the coatings before and after annealing. (a) Tests are operated dispersedly on the surface and designedly on the cross-section, both of that are performed for 3 times. (b) Compositional change of the B and C shows that B diffuses to the B rich region while C goes to the exterior with the increase of the annealing temperature.

annealed at 1600 °C is mainly composed of PyC and dispersive B_4C nano-grains. The PyC is a natural barrier to prevent grain growth of B_4C to a certain degree. However, the grain boundary of B_4C is still migrated and enlarged by absorbing B and C from the metastablely B-doped PyC and also by devouring those smaller crystals with higher surface energies at elevated annealing temperatures. Some B_4C grains (Fig. 5c) grow to a large size of approximately 500 nm after annealing at 2000 °C. More stacking faults are formed in larger grains to release the residual stress caused by collision, and to harmonize the un-released stress induced by heating and cooling. SAED pattern reveals that the orientation of the stacking faults is parallel to the (0$\bar{1}$1) plane of B_4C, identified by the elongation of the (0$\bar{1}$1) diffractions. Besides, Raman spectrum is investigated to characterize the annealing-induced change of the PyC structure (Fig. 6a). R is defined as the graphitization degree, the value of that is calculated by the intensity of

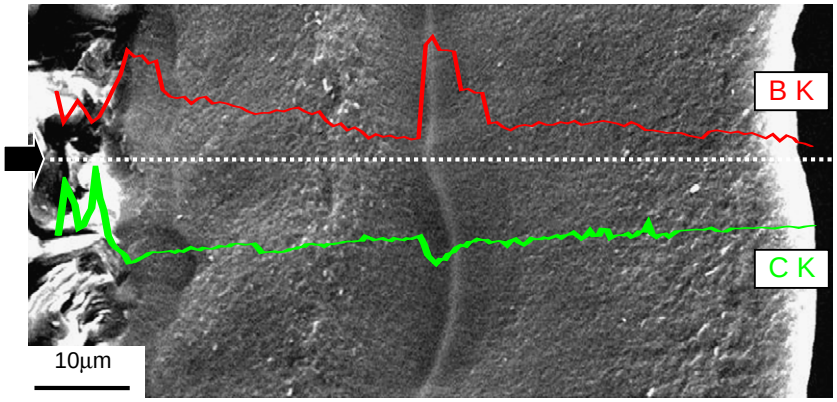

Fig. 7. EDS line scanning results of B (red line) and C (red line) on cross-section of the as-deposited coating indicate notable composition gradients along the coating thickness. (For interpretation of the references to color in this figure legend, the reader is referred to the web version of this article.)

D bond (disordered PyC) divided by that of the G bond (graphite PyC). The formula is as follows:

$$R = I_D / I_G.$$

Apparently, R value changes in a reverse trend to the intensity of the G bond (I_G), and therefore to the graphitization degree. Result shows that the graphitization of PyC is clearly enhanced with the elevated temperature (Fig. 6b) as R decreases from 3.4 (unannealed coating) to 1.3 (annealed at 2000 °C for 2 h). The quantification of PyC graphitization is meaningful for controlling the coating microstructure accurately by changing the annealing conditions. It is noteworthy that the PyC becomes more ordered at the interface of the B_4C/PyC, and makes an extension with (002) planes along the low miller indices plane of the B_4C crystal to form an epitaxial structure (Fig. 5d). Limited by the thermal activation energy, the extension only keeps for about 5 nm.

3.4. Compositional analysis

EDS is a proper technique for determining element content of above 0.5 at.% in select-sized area. The minimum content tested (C at.% in the coating cross-section after annealing at 2000 °C) in this experiment is about 15 at.%, which means that the compositional evolution of B and C can be studied effectively using EDS, although the B and C are relatively difficult to be detected than those heavier elements. Distribution of B and C in the as-deposited coating is investigated and shown in Fig. 7. Evident gradients are identified along the coating thickness. Interface between the two layers has the maximum B content. The high concentration keeps for about 5 μm in distance and then declines dramatically to a stable level. C shows an opposite trend as B does. Moreover, a similar compositional variation is observed from the layer/substrate interface to the layer/layer interface. It seems that the source gas of B is relatively easy to be absorbed than that of C to form a B rich region at each beginning of the two depositions, which has less to do with the deposited substrates. The absorption is saturated within a certain time as a relatively uniform composition is formed with an unconspicuous B reduction toward the exterior. Formation of the composition gradients may result from temperature difference between the initial heating and the heat preserving in each deposition. It may also relate to the presence of a higher energy barrier of CH_4 than that of BCl_3 in the decomposition and gas phase reaction of the CVD process [16].

According to the theory of diffusion kinetics and thermodynamics, the grain growth of B_4C could be attributed to the diffusion of C and B in the solid phase [29]. A scheme is designed specially to explore the diffusion rule induced by the high temperature annealing, as shown in

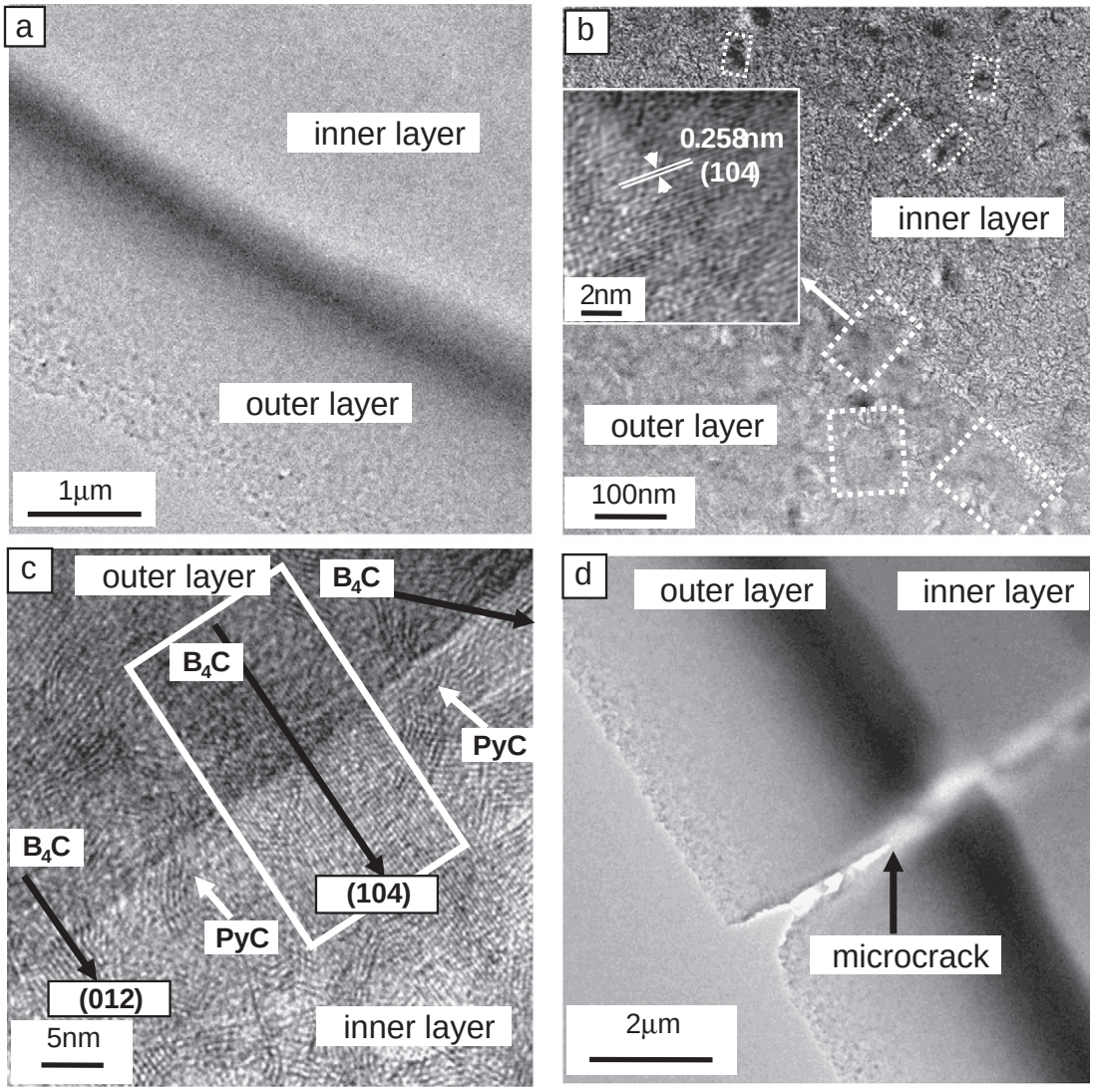

Fig. 9. Microstructure of the two-layer coating annealed at 1600 °C. (a) BF image of the coating, (b) microstructure differences between the two regions separated by the layer/layer interface, (c) epitaxial growth of the B_4C crystallites, (d) microcrack penetrates the layer/layer interface with no deflection.

Fig. 8. For each specimen, element concentration is measured 3 times both on the surface and cross-section. A magnification of 10,000× is used in the cross-sectional test for getting the average content of the outer coating in an area of $25 \times 20\ \mu m^2$ (several micrometers are left from the surface). The depth of characteristic X-ray signal in the EDS test is approximately 2 μm, which means that the designed cross-sectional test provides convictive information of the inner coating without interference of the surface results. Compositional evolution of the annealed coating is shown in Fig. 8b. A decrease of the B content and an increase of the C content are induced on the coating surface after annealing. Nevertheless, totally reversed trends of the B and C content to that of the surface test are identified on the coating cross-section. It indicates that B diffuses towards the B rich region while C goes to the exterior during the heating process. As a result of the diffusion, a larger concentration gradient is formed than the one existing in the as-deposited coating. TEM is applied to determine the microstructure evolution induced by the element diffusion. The dark part between the two layers in Fig. 9a represents the B rich region. Fig. 9b shows obviously different structures in the two regions separated by the layer/layer interface. The B rich region is mainly composed of grown B_4C, while the inner layer (near the layer/layer interface) is made of PyC and dispersed B_4C crystallites. The grain size of B_4C in the inner layer is much smaller than that in the B rich region. Moreover, epitaxial growth of B_4C at the layer/layer interface is identified by the HR image (Fig. 9c), in which the matrix crystals belong to the B rich region while the growing ones belong to the inner α-B_4C layer. It can be deduced that the B rich region possesses faster crystallization rate due to the more appropriate B/C mole ratio close to that of B_4C. While, the B_4C crystallites separated out of the inner layer grow on those grown ones in the B rich region along low miller index planes. Since the preferential crystallization is stochastic and non-oriented, the later precipitated crystals cannot grow along the same crystal orientation. As is shown by the TEM images, the microstructure of the annealed coating becomes more asymmetrical than that of the as-deposited one especially at the layer/layer interface, which resulted from the difference in the crystallization rate of B_4C induced by the evident B/C gradient. However, the bond of the layer/layer interface is enhanced after annealing. Microcracks can penetrate the interface without deflection (Fig. 9d). Performances of the B–C coating modification on CMCs were given great interest and explored. Studies showed that a weak bond between the matrix coatings could result in interfacial debonding, which was beneficial to improve the mechanical properties of the CMCs [30]. Further research [31–33] revealed that the mechanical properties could get better as stronger bond was formed at the interface of the matrix/interphase (the interphase is always turbostratic boron nitride or pyrolytic carbon), since cracks were kept and propagated within the stratified structure of the interphase to consume more energy. It seems that varying mechanical properties are required for the CVD boron carbide coatings when they serve as different CMC components in different locations. Proper coating performance can be obtained by controlling the microstructure through changing the annealing conditions. A mechanism is proposed to show the structural

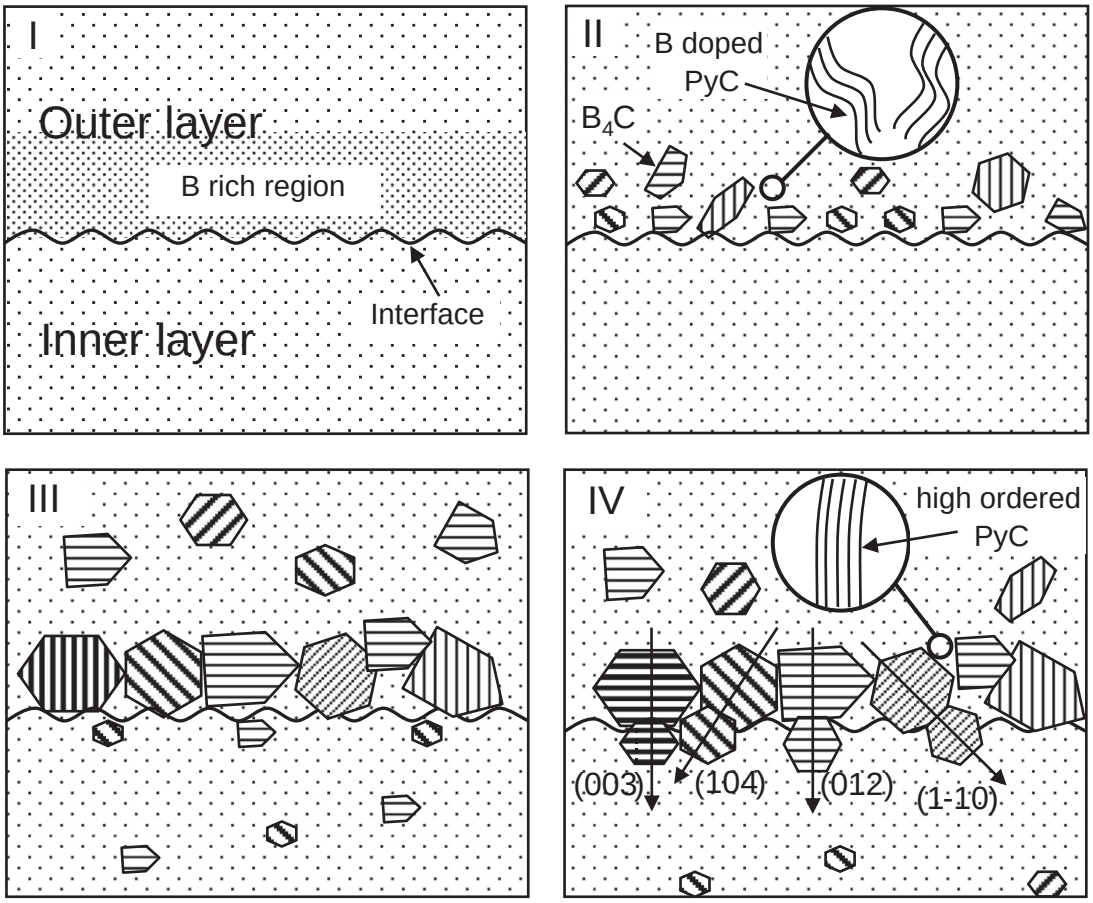

Fig. 10. Microstructural evolution mechanism of the two-layer coating annealed at high temperatures. (I) Composition gradients of B and C have been induced in the as-deposited coating by CVD, (II) B_4C crystallites precipitate early out of the B rich region and (III) grow faster in the heating process, (IV) the later precipitated B_4C crystallites in the inner layer at the layer/layer interface grow on the grown B_4C in the B rich region along low miller index planes.

evolution of the two-layer coating induced by annealing at high temperatures up to 2000 °C, as shown in Fig. 10. There are mainly four steps concerned: (I) A compositional gradient of B and C is intrinsically induced in the as-deposited α-B_4C coatings by CVD, (II) B_4C crystallites precipitate preferentially out of the B rich region and (III) grow faster than other regions in the heating process by receiving B and C from B doped PyC. The grain coarsening is inhibited by PyC as doping B is depleted, (IV) the later precipitated B_4C crystallites in the inner layer at the layer/layer interface grow epitaxially along the low miller index planes of the grown B_4C in the B rich region. However, many aspects remain to be explored about the correlation of microstructure and mechanical properties.

4. Conclusions

A two-layer α-B_4C coating has been deposited and annealed at high temperatures from 1600 °C to 2000 °C. Study on microstructure reveals that the as-deposited coating is composed of low ordered PyC and α-B_4C with notable composition gradients of B and C along the coating thickness, C varies in the opposite trend as B does. After annealing at 1600 °C, α-B_4C partly turns as B_4C crystallites, which are enlarged subsequently by receiving B and C from B-doped PyC under elevated temperatures. Much higher concentration gradient of B and C is formed after annealing as the temperature rises up to 2000 °C. The B rich region crystallizes faster than other regions due to the suitable B/C mole ratio close to that of B_4C. TEM identifies an epitaxial growth of B_4C controlled by the difference in the crystallization rate at the layer/layer interface. Bond of the layer/layer interface is enhanced after annealing.

Acknowledgement

This work was financially supported by the National Natural Science Foundation of China (No. 90405015 and No. 50532010).

References

[1] K. Kobayashi, K. Miyazaki, I. Ogawa, T. Hagio, H. Yoshida, Mater. Des. 9 (1988) 10.
[2] L. Quemard, F. Rebillat, A. Guette, H. Tawil, C. Louchet-Pouillerie, J. Eur. Ceram. Soc. 27 (2007) 2085.
[3] J. Bouix, C. Vincent, H. Vincent, R. Favre, Mater. Res. Soc. Symp. Proc. 168 (1990) 305.
[4] H. Vincent, H. Mourichoux, J.P. Scharff, C. Vincent, J. Bouix, Thermochim. Acta 182 (1991) 253.
[5] M. Bouchacourt, F. Thevenot, J. Less-Common Met. 67 (1979) 327.
[6] M. Beauvy, J. Less-Common Met. 90 (1983) 169.
[7] K.A. Schwetz, P. Karduck, J. Less-Common Met. 175 (1991) 1.
[8] U. Jansson, J.O. Carlsson, B. Stridh, J. Vat. Sci. Technol. 5 (1987) 2823.
[9] K. Ploog, J. Cryst. Growth 25 (1974) 197.
[10] U. Jansson, J.O. Carlsson, Thin Solid Films 124 (1985) 101.
[11] D.N. Kevill, T.J. Rissmann, D. Brewe, C. Wood, J. Cryst. Growth 74 (1986) 210.
[12] L. Vandenbulcke, R. Herbin, M. Basutcu, J.N. Barrandon, J. Less-Common Met. 80 (1981) 7.
[13] L. Vandenbulcke, Ind. Eng. Chem. Process Des. Dev. 24 (1985) 568.
[14] S.N. Dilek, H.O. Ozbelge, N.A. Sezgi, T. Dogu, Ind. Eng. Chem. Res. 40 (2001) 751.
[15] U. Jansson, J.O. Carlsson, B. Stridh, S. Soderberg, M. Olsson, Thin Solid Films 172 (1989) 81.
[16] T.S. Moss, W.J. Lackey, K.L. More, J. Am. Chem. Soc. 81 (1998) 3077.
[17] J. Berjonneau, G. Chollon, F. Langlais, J. Electrochem. Soc. 153 (2006) 795.
[18] Y.S. Liu, L.T. Zhang, L.F. Cheng, Q.F. Zeng, W.H. Zhang, W.B. Yang, Z.D. Feng, S.W. Li, B. Zeng, Appl. Surf. Sci. 255 (2009) 5729.
[19] B. Zeng, Z.D. Feng, S.W. Li, Y.S. Liu, L.F. Cheng, L.T. Zhang, Ceram. Int. 35 (2009) 1877.
[20] T. Shirasaki, A. Derre, M. Me´ne´trier, A. Tressaud, S. Flandrois, Carbon 38 (2000) 1461.
[21] M. Olsson, S. Soderberg, B. Stridh, U. Jansson, J.O. Carlsson, Thin Solid Films 172 (1989) 95.
[22] C.T. Hach, L.E. Jones, C. Crossland, P.A. Thrower, Carbon 37 (1999) 221.
[23] W.A. Yarbrough, J. Am. Ceram. Soc. 75 (1992) 3179.
[24] S. Jacques, A. Guette, X. Bourrat, F. Langlais, C. Guimon, C. Labrugere, Carbon 34 (1996) 1135.
[25] H. Kunzli, P. Gantenbein, R. Steiner, P. Oelhafen, J. Nucl. Mater. 196 (1992) 622.
[26] C. Ronning, D. Schwen, S. Eyhusen, U. Veter, H. Hofsass, Surf. Coat. Technol. 158 (2002) 382.
[27] L.G. Jacobsohn, R.K. Schulze, M.E.H. Maia da Costa, M. Nastasi, Surf. Sci. 572 (2004) 418.
[28] W. Cermignani, T.E. Paulson, C. Onneby, C.G. Pantano, Carbon 33 (1995) 367.
[29] H. Vincent, C. Vincent, M.P. Berthet, J. Bouix, G. Gonzalez, Carbon 34 (1996) 1041.
[30] C. Lacroix, D. Leguillon, E. Martin, Compos. Sci. Technol. 62 (2002) 519.
[31] T. Hinoki, W. Yang, T. Nozawa, T. Shibayama, Y. Katoh, A. Kohyama, J. Nucl. Mater. 289 (2001) 23.
[32] F. Rebillat, J. Lamon, A. Guette, Acta Mater. 48 (2000) 4609.
[33] S. Bertrand, C. Droillard, R. Pailler, X. Bourrat, R. Naslain, J. Eur. Ceram. Soc. 20 (2000) 1.